Materials Characterization 191 (2022) 112162

Contents lists available at ScienceDirect

Materials Characterization

journal homepage: www.elsevier.com/locate/matchar

Comparative study of additively manufactured and reference 316 L stainless steel samples – Effect of severe shot peening on microstructure and residual stresses

Tejas Gundgire [a,*], Tuomas Jokiaho [a], Suvi Santa-aho [a], Timo Rautio [b], Antti Järvenpää [b], Minnamari Vippola [a]

[a] Tampere University, Materials Science and Environmental Engineering, P.O 589, 33100 Tampere, Finland
[b] Kerttu Saalasti Institute, University of Oulu, Pajatie 5, 85500 Nivala, Finland

ARTICLE INFO

Keywords:
Additive manufacturing
Selective laser melting
Stainless steel 316 L
Residual stresses
Post processing
Shot peening

ABSTRACT

The as-built selective laser melted (SLM) austenitic stainless steel 316 L components are characterized by presence of quality related concerns such as tensile residual stresses, poor surface finish, etc. These issues may prove to be detrimental during the actual usage of components and could result in poor mechanical performance. Therefore, it is important to perform the apt post processing such as heat treatment and shot peening to tailor such problems and facilitate improved mechanical performance. In the present work, additively manufactured (AM) 316 L samples were subjected to shot peening with different parameters including the severe shot peening (SSP) procedure. The identical shot peening protocol was also applied to reference samples to evaluate the comparable response. Both the shot peened reference and AM samples were studied for residual stresses, surface topography, microhardness, and the corresponding microstructure. The results indicated, that SSP induced higher values of compressive residual stresses deeper into the samples. This was accompanied by reduced surface roughness, increased grain refinement depth, and higher microhardness near the surface. The SSP resulted in transformation of original austenite to martensite near the surface in the reference samples.

1. Introduction

Selective laser melting (SLM) is a metal additive manufacturing (AM) method which facilitates production of intricate geometries, reduction in overall weight of the components, etc. [1,2]. In SLM, A laser beam is used as an energy source to melt and fuse the metal powder in layer-by-layer fashion to build the final component [3]. Even though several metal alloys can be manufactured with SLM, 316 L stainless steel is of great interest because of its excellent corrosion resistance, high strength, and biocompatibility [4]. The aforementioned properties enable the use of 316 L stainless steel in various industries including aerospace, biomedical, nuclear as well as ship manufacturing [5]. However, the as printed SLM 316 L stainless steel components are characterized by inevitable concerns such as presence of detrimental tensile residual stresses and rougher surface which could negatively affect the mechanical and stress corrosion performance during actual working operation in challenging environments [6]. Therefore, an apt post processing protocol must be applied to achieve the desirable mechanical performance.

Residual stress formation is unavoidable in SLM processing of 316 L parts because of the lower process temperature compared to electron beam melting (EBM), higher temperature gradients, rapid cooling rates and remelting of previous layers leading to complex heating and cooling cycles [6,7]. When laser beam melts the powder, the melted material expands against the underlying layers inducing the compressive residual stresses. Furthermore, rapid cooling enabled by higher temperature gradients result in material shrinkage inhibited by already deposited layers resulting in formation of tensile residual stresses [7–10]. Several efforts are being made to control the formation of these complex and detrimental residual stress fields by optimizing various process parameters [7,11]. Furthermore, usually, a stress relief heat treatment is performed on as-built SLM 316 L parts to relieve these residual stress fields [12]. Moreover, further tailoring of the near surface residual stresses could be done with post processing methods such as laser shock peening, shot peening, etc. [6]. Shot peening induces beneficial compressive residual stresses on surface and subsurface. Presence of relatively large

* Corresponding author.
E-mail address: tejas.gundgire@tuni.fi (T. Gundgire).

https://doi.org/10.1016/j.matchar.2022.112162
Received 28 February 2022; Received in revised form 15 July 2022; Accepted 23 July 2022
Available online 27 July 2022

compressive residual stresses on surface and beneath could assist in improvement of fatigue performance [13]. To achieve such stresses, severe shot peening (SSP) could be used. SSP is an intensive shot peeing protocol applying increased kinetic energy or increasing exposure time of peening media. Previous studies reported increased compressive stresses which extended deeper from the surface when conventionally manufactured 316 L and 304 stainless steels were subjected to SSP [14,15].

In addition to higher and deeper compressive residual stresses, the surface properties of the AM samples could be significantly improved with SSP. The surface of as processed SLM 316 L samples is usually rough. Efforts have been made to improve the surface finish by using the optimal combination of process parameters [16–18]. However, further improvement could be facilitated by subjecting the samples to appropriate shot peening. Previously, Rautio et al. [19] reported improvement in roughness values of as built SLM AlSi10Mg when subjected to a glass bead shot peening. Furthermore, for the conventionally built austenitic stainless steels, SSP has been proven effective in enabling heavy plastic deformation and thus grain refinement deeper into the samples surface when compared to the conventional shot peening [14,15]. Previously Bagherifard et al. [14] reported presence of nano and sub-micron sized grains when conventionally manufactured AISI 316 L stainless steel was subjected to SSP. SSP can also enable the deformation induced phase transformation of austenite to martensite on the surface [15]. SSP induced work hardening, grain refinement as well as martensitic phase transformation can result in improved hardness in near surface areas [14]. Even though SSP of conventionally manufactured austenitic steels is well known [14,15], the SSP response of AM 316 L is still a work in progress. The AM processed 316 L stainless steel possess different microstructure as well as surface properties when compared to conventionally manufactured steels. Therefore, it is important to study the effect of SSP on AM manufactured 316 L and also relate/compare with the well-known SSP response of conventionally manufactured 316 L steel. Moreover, with the defects being mainly concentrated in near surface areas of SLM built 316 L [20–22], surface and subsurface enhancements achieved from SSP could form the basis for the improved mechanical performance especially within fatigue and/or stress corrosion cracking.

In the present study, additively manufactured (AM) 316 L samples were subjected to shot peening with different parameters. Some of the parameters imitated the SSP protocol with 22 and 42 number of passes. The SSP term utilized in this study refers to increased time scale of shot peening process to achieve the highest surface modifications possible. The time scale in this study is calculated as number of shot peening nozzle passes. Similar sized conventionally manufactured reference samples were also subjected to identical shot peening parameters as that of AM samples. The shot peened AM as well as reference samples were comprehensively characterized for microstructure including surface topography and roughness, phases, surface and subsurface residual stresses, grain refinement and microhardness. A comparable response of AM and reference samples when subjected to identical shot peening parameters is presented in this work based on aforementioned characterization.

2. Materials and methods

2.1. SLM built 316 L and REF samples

Spherical shaped powder supplied by Carpenter Additive (United Kingdom) was used in the present study. The powder particle size was 15–45 μm and had a chemical composition as shown in the Table 1. The AM specimens were built in a SLM solution's SLM 280HL machine situated at University of Oulu, Finland. The size of each specimen was 80 × 20 × 2 mm. The standard printing parameters recommended by the machine supplier were used to build the samples. The printing chamber was preheated and kept constant at 150 °C throughout the printing process. The laser power of 200 W was used with a scanning speed of 800 mm/s. The layer thickness was 30 μm and the hatch spacing was 120 μm. The as-printed samples were subjected to stress relief annealing heat treatment at 600 °C for 2 h in a muffle furnace (Sarlin 1000HS-436). Similar sized (80 × 20 × 2 mm) reference samples were cut from a 2 mm thick AISI 316 L stainless steel sheet (EN 1.4404).

2.2. Shot peening

Additively manufactured as well as reference samples were subjected to shot peening with different parameters. Martensitic chromium media with hardness of 42 HRC and particle size of 0.40–0.85 mm was used. A 6-axis industrial robot along with shot blasting pot and nozzle were used in a close cabinet to perform the experiments. The samples were blasted with optimum nozzle distance of 70 mm with a pressure of 7.4 bar. The Almen intensity measurement process was conducted according to [23]. The time scale of measurements was calculated as number of passes of the nozzle. Authors found use of number of passes for finding the Almen intensity to be most practical to achieve the repeatability of the process as well utilizing the shot peening for different kind of specimens. The intensity was determined with type A strips and the Almen saturation intensity was found to be 240A. Detailed description of the shot peening experiments have been earlier reported elsewhere by the concerned group [24].

Five different samples with different number of passes were used with two different nozzle diameters. The shot peening parameters along with samples designations are listed in Table 2. All the AM samples were heat treated prior to shot peening. Table 2 shows the shot peening parameters of additively manufactured + heat treated (AMHT), additively manufactured + heat treated + shot peened with 1 pass (AM1). AM2, AM4, AM22 and AM42 follow the similar terminology as that of AM1. Shot peening with 22 and 42 number of passed was considered as severe shot peening (SSP) in this work.

Table 2
Shot peening parameters.

Manufacturing method	Designation	Shot peening passes	Shot peening nozzle speed (mm/s)	Corresponding number of passes for 50 mm/s speed
SLM built	AMHT	0	0	0
	AM1	1	50	1
	AM2	2	150	0.67
	AM4	4	150	1.33
	AM22	22	50	22
	AM42	42	150	14
Reference	REF	0	0	0
	REF1	1	50	1
	REF2	2	150	0.67
	REF4	4	150	1.33
	REF22	22	50	22
	REF42	42	150	14

Table 1
Chemical composition of 316 L powder used in this work.

Element	Fe	Cr	Ni	Mo	Mn	Si	C	Cu	O	N	S	P
wt. %	bal.	17.6	12.5	2.38	0.66	0.65	0.02	0.02	0.03	0.09	0.006	0.007

2.3. Microscopic characterization and surface roughness measurement

The samples were cut and ultrasonically cleaned in ethanol for the topographic analysis. For the cross-sectional analysis, the samples were cut along the cross section and were hot mounted in a conductive thermosetting resin called PolyFast. Mounted specimens were then ground with 320, 500, 1200 and 2000 SiC papers followed by diamond polishing with suspension size of 3 μm and 1 μm on Tegramin 30 (Struers, Denmark) polisher. The cross-sectional samples were etched with a V2A etchant composed of water, hydrochloric acid, and nitric acid in 10:10:1 ratio. The etchant was first heated until the fumes were visible with naked eyes followed by sample immersion in solution for 10 s. Both topographic as well as cross sectional microstructural characterization was performed on JSM IT 500 (JEOL, Japan) scanning electron microscope and a field emission scanning microscope (FESEM) ULTRAplus (Zeiss, Germany). The surface roughness measurements were performed using a 3D optical profilometer (Alicona InfiniteFocus, G5, Austria). The area of 4 mm × 4 mm was scanned using a 10× objective magnification. The average roughness of profile (Ra) was derived by drawing a zigzag line of 40 μm over the scanned area. The mean peak to valley height of roughness profile (Rz) values were also derived and they followed the similar trend as that of Ra values. Therefore, only Ra values are reported here for the sake of brevity.

Similar polishing protocol was followed to prepare the samples for electron backscatter diffraction (EBSD) measurements. In addition to previous steps, 1 μm diamond polishing was followed by 0.05 μm colloidal silica suspension. The EBSD system by Oxford instruments (United Kingdom) combined with FESEM was used for the measurements. Fine scans of 100 × 30 μm were performed with a step size of 70 nm from the near surface layers. The Aztec software was used for data collection while the CHANNEL 5 software was used to generate the inverse pole figure (IPF) as well as phase maps.

2.4. Phase identification and RS measurements

Phase identification was made by a multipurpose X-ray diffractometer (PANalytical B. V., Netherlands). Measurements were carried out by the CoKα radiation source with power settings of 45 mA current and 40 kV voltage. The 2θ range of 26° to 96° with a step size of 0.026° was set for the measurements. Highscore^{+} software was used for the post measurement analysis to identify the phases. The software uses the available database of the international centre for diffraction data to compare the existing data with previously available one.

Xstress 3000 (Stresstech Oy, Finland), an X-ray diffractometer which uses modified chi method and is based on X-ray diffraction mechanism was used for the residual stress (RS) measurements. The equipment has two X-ray detectors placed symmetrically on the either side of the goniometer impinging the incident beam. The modified chi method measures and calculates the inter planar lattice distances. These spacings could be either stretched out or compressed based on the type of residual stress field present at the measured location [25]. Measurements were done with a 3 mm diameter collimator and a manganese (Mn) tube with diffraction angle of 152.3°. The residual stresses were measured in both the longitudinal (0) as well as tangential (90) direction (refer Fig. 1). First, surface residual stresses were measured as a preliminary investigation at four different locations as indicated on the Fig. 1. These locations had no significant difference in residual stress values. Therefore, location 1 and 3 were selected for the depth profile measurements. A MoviPol-5 electrolytical polisher (Struers, Denmark) was used to selectively remove the material for the residual stress depth profile measurements. The electrolyte used was A2 which composed of perchloric acid and ethanol. Electrolytic polishing has been proven reliable method for the measurement residual stress depth profile [26,27]. The depth of material removed after each step was measured using a dial gauge (Mitutoyo, Japan). Two depth profiles measured at location 1 and 3 exhibited similar trend and values and hence depth profiles at location 3 are reported in results.

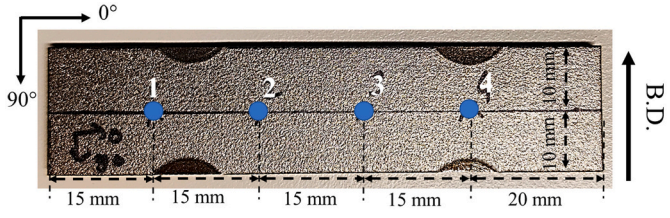

Fig. 1. Residual stress measurement directions. The arrow on the right indicates building direction for AM samples.

2.5. Microhardness

The microhardness was measured along the cross section of the samples starting from 25 μm depth from the surface. The equipment used for the measurements was MMT-X7 (Matsuzawa, Japan). The load used was 0.05 kg and difference between each measurement was 50 μm. The process was repeated for three times for each sample.

3. Results and discussion

The AM as well as reference samples were subjected to shot peening with different process parameters and were investigated for morphology, surface roughness, residual stresses, grain structure and microhardness. The investigated findings are presented and discussed comprehensively in this chapter.

3.1. Topographic and cross-sectional morphology

3.1.1. Reference samples

Fig. 2(a-f) and (a′-f) shows the topographic and the cross-sectional morphologies of the un-peened and shot peened reference samples described in Table 2. The REF 316 L steel typically exhibits the equiaxed grain morphology and not so wavy surface as shown in Fig. 2(a-a) [28]. It can be clearly seen from the figure that the shot peening has induced a surface waviness on the top of the samples. The bombardment of shot peening media impinges indents on the surface and induces waviness. There is no significant difference in the waviness exhibited by the samples REF 1, REF 2 and REF 4 (Fig. 2(b-c-d)). However, severely peened samples REF 22 and REF 44 have reduced surface waviness compared to them. The severe bombardment again evens out the indentations to some extent to again reduce the waviness. Shot peening induced the indentation overlaps as indicated in the Fig. 2(d). The indentation overlaps seem to be increasing with increasing number of passes. The presence of particle like structures could be seen in severely peened samples REF 22 and REF 42 (Fig. 2(e-f)). Those are indicated by the black arrows. Similar observations were made previously for the severely shot peened commercial 304 stainless steel [15].

3.1.2. AM samples

The high thermal gradients, complex heating and cooling and complicated metallurgical process leads to formation of distinct microstructure in SLM built 316 L parts compared to conventionally manufactured steels [29]. The typical microstructure of SLM built 316 L stainless steel comprised of half cylindrical melt pools and cellular structure as shown in Fig. 3(a-c).

Fig. 4(a-f) and (a′-f) shows the topographic and the cross-sectional morphologies of the un-peened and shot peened AM samples described in Table 2. The laser melted tracks are clearly visible in the as-built heat treated (AMHT) sample. Presence of un-melted and spattered spherical particles can also be seen from the Fig. 4(a – a). Various process parameters such as scanning speed, layer thickness could affect the formation of such particles which create irregularities on the surface

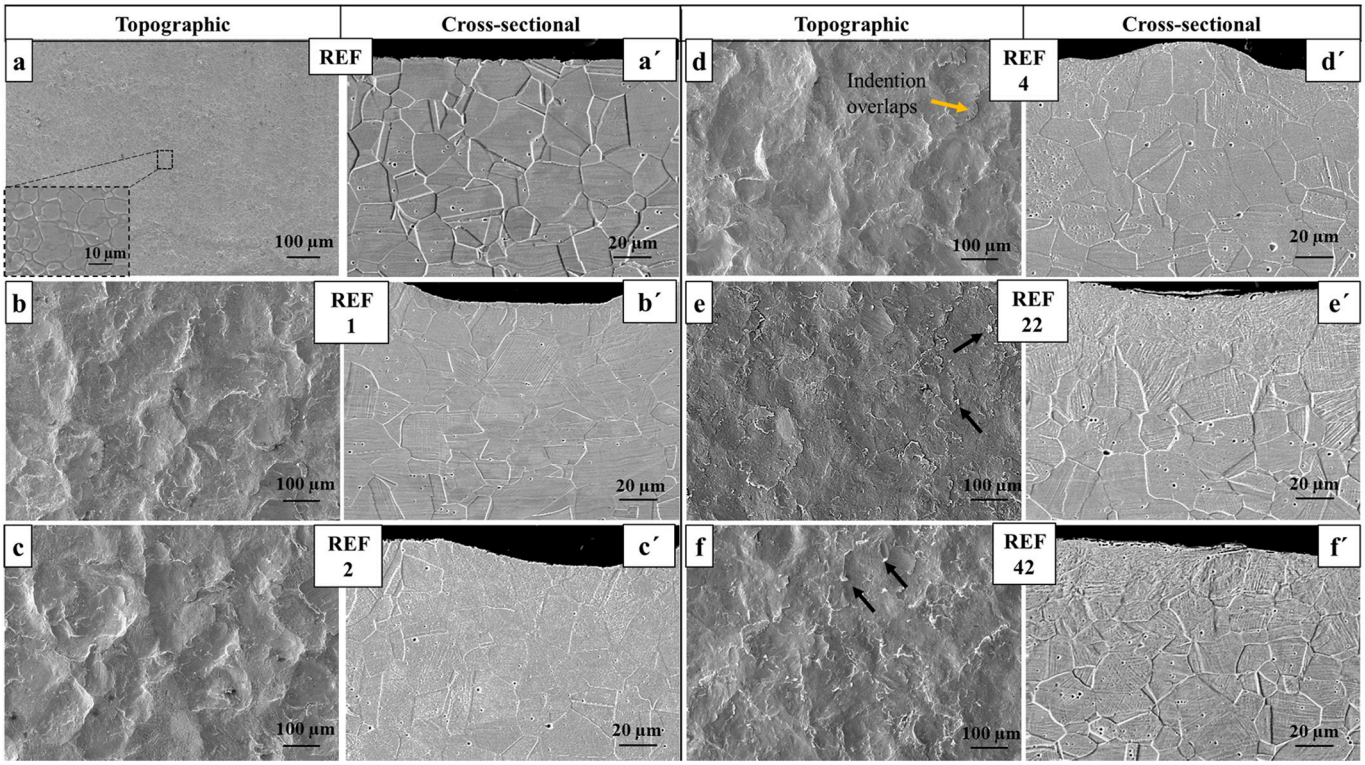

Fig. 2. Topographic and cross-sectional micrographs of shot peened reference samples respectively a, a) REF; b, b) REF 1; c, c) REF 2; d, d) REF 4; e, e) REF 22; f, f) REF 42.

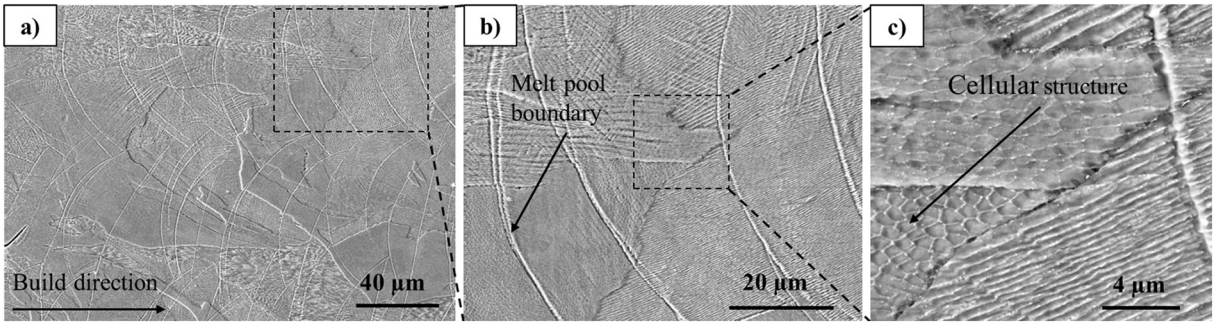

Fig. 3. Microstructure of as-printed AMHT samples observed from the cross-section (2 mm thick side).

[17,30]. Subjecting the AM samples to shot peening reduced surface irregularities to some degree. Shot peening with 1, 2 and 4 number of passes have almost evened out these spherical particles on surface. However, some of such particles were still present on surface and can be seen from Fig. 4(b-c-d) (b́-ć-d́). Furthermore, 22 and 42 number of passes completely evened out those particles on the surface, making the surface less wavy (Fig. 4(e-f; é-f́)). Among the shot peened samples, indentation overlaps have increased with increasing number of passes. Furthermore, presence of particle like structures can be seen from Fig. 4(e-f) with 22 and 42 number of passes. Previously Liu et al. [15] has reported presence of similar particles on surface of conventionally manufactured 304 stainless steel when subjected to severe shot peening.

To summarize, the cross-sectional analysis depicts that the surface quality of the as-printed SLM sample had irregular surface unlike the un-peened REF sample. This could be attributed to overlapping of the half cylindrical melt pools on each other during SLM processing of 316 L thereby resulting in irregular surface. Moreover, the un-melted spherical powder particles attached to surface by capillary action in the melt pool also contribute to these surface irregularities in SLM 316 L parts. Shot peening affects differently to AM samples as that of reference samples mainly because of starting surface. In case of REF sample, the un-peened surface was almost flat with few irregularities. Shot peening first induced surface waviness and SSP reduced it by a little margin. Because un-peened AMHT surface had high irregularities, shot peening first reduced them and SSP again reduces it. Indentations overlaps increase with increasing number of passes in both REF and AM samples with highest being in SSP samples. Furthermore, particle like structures were observed with SSP of both REF and AM samples.

3.2. Roughness measurement

3.2.1. Reference samples

The 3-dimensional (3D) topographic images of un-peened as well as peened reference samples are shown in Fig. 5(a-f). The surface roughness values derived from the 3D topographic images are indicated in Fig. 5(g). The un-peened reference sample was relatively smooth (Fig. 5 (a)) and had average surface roughness value (Ra) of 0.23 ± 0.001 µm. The sample is indicated by a dot in the Fig. 5(g) as it was not clearly

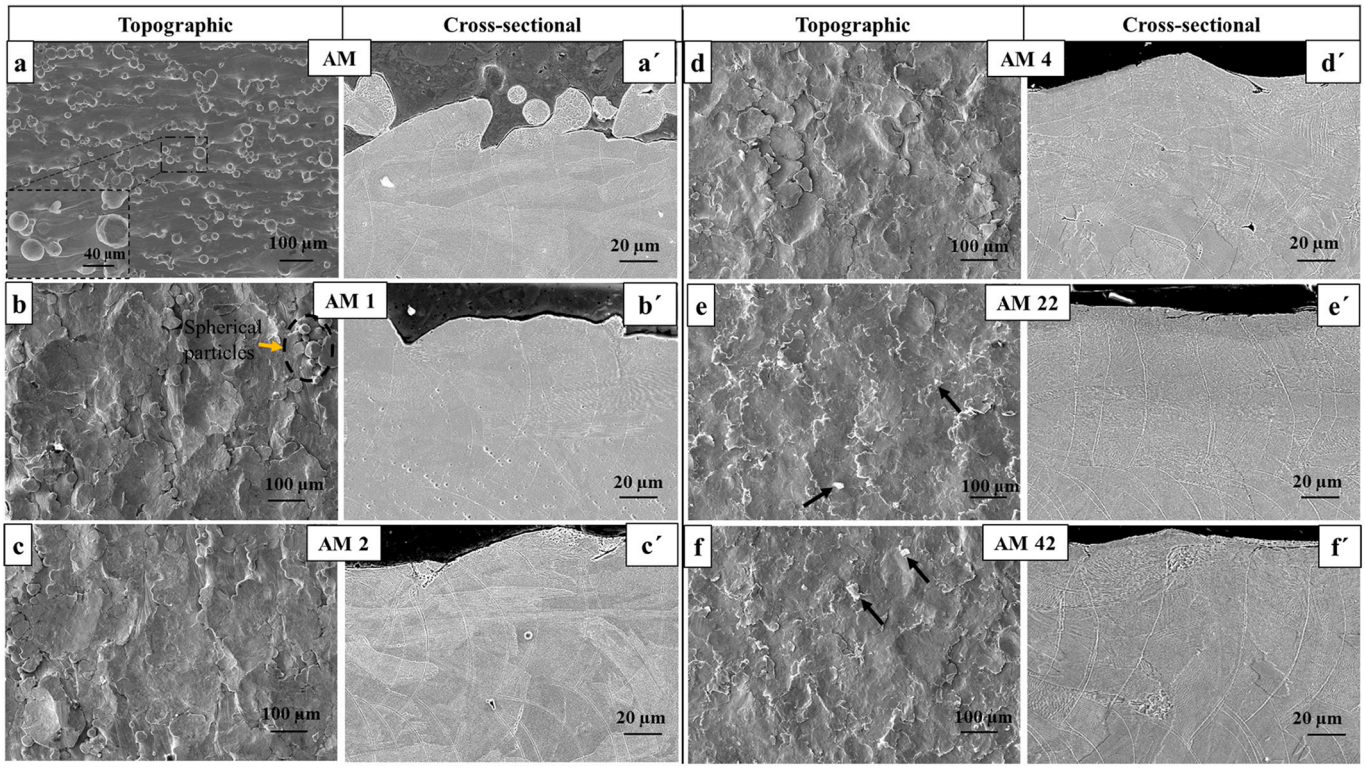

Fig. 4. Topographic and cross-sectional micrographs of shot peened AM samples respectively a, a) AMHT; b, b) AM 1; c, c) AM 2; d, d) AM 4; e, e) AM 22; f, f) AM 42.

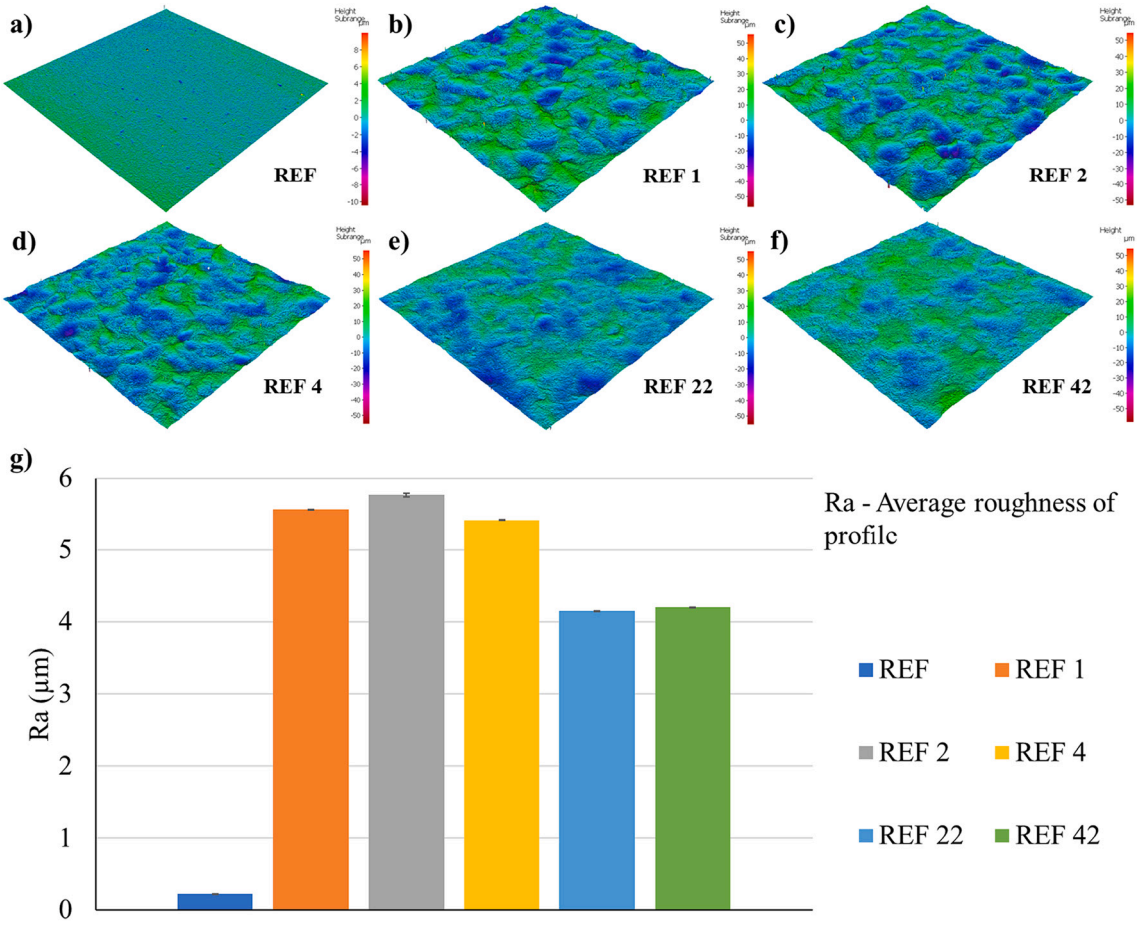

Fig. 5. a-f) 3D topographic images of reference samples; g) Surface roughness of the reference samples derived from the corresponding topographic images.

visible. Shot peening increased the surface roughness (Ra) by a significant value i.e., from 0.23 μm in un-peened sample to 5.57 μm in REF 1 sample with just 1 pass, which can be visualized from Fig. 5(a-b). Shot peening media induces indentations on the surface of sample which results in producing rougher surface [15]. The roughness values of REF 2 and REF 4 are closer to the roughness value of REF 1 and it can be visualized from Fig. 5(b-c-d). However, the roughness (Ra) values were reduced to 4.15 μm and 4.20 μm with 22 and 42 number of passes in REF 22 and REF 42 respectively. Severe bombarding of shot peening media again reduces the roughness by a small amount [15], which can be visualized from Fig. 5(d-e-f).

3.2.2. AM samples

The 3-dimensional (3D) topographic images of un-peened as well as peened AM samples are shown in Fig. 6(a-f). Surface roughness values derived from the 3D topographic images are indicated in Fig. 6(g). The surface of un-peened AMHT sample was rough and had Ra value of 8.81 μm. Previously discussed surface waviness or irregularity caused due to presence of spherical particles on surface of AMHT sample can be clearly visualized from Fig. 6(a). In AM processing of 316 L steel, the surface roughness is dependent on the tuning of various process parameters. Low energy density results in formation of cracks, pores and spherical particles on surface [17]. Faster scanning speeds could negatively affect the surface quality of AM samples [18,31]. Furthermore, layer thickness, scan speed, etc. could also impair the surface quality. These aforementioned surface irregularities could be minimized by optimizing the process parameters but cannot be completely eliminated [16]. Shot peening with just 1 pass improved the surface quality significantly (Ra = 5.81 μm) and can be clearly visualized from Fig. 6(b). Shot peening with 2 (6.06 μm) and 4 (5.3 μm) number of passes did not have significant effect when compared to that with 1 pass. However, the surface seems to be evened out with 22 and 42 number of passes from Fig. 6(e-f) when compared to 4 number of passes. That is also evident from the surface roughness values i.e., Ra value of 5.3 reduced to 3.93 and 3.87 with 22 and 42 number of passed respectively.

To summarize, the response of reference and AM samples to the shot peening in terms of surface roughness depends on the starting roughness values of the corresponding samples. The un-peened REF sample was relatively smooth, and first shot peening increased the roughness by a significant value and then SSP again reduced it by a small value. However, the un-peened AMHT sample was relatively rough. Therefore, the shot peening first reduced the roughness by a significant value while SSP again reduced by a small value.

3.3. Phase analysis and residual stress

3.3.1. XRD phase analysis

The XRD profiles for the reference and AM samples are presented in Fig. 7(a) and (b) respectively. The resolved peaks are indicated as austenite and martensite on the figure. Reference samples shot peened with 1, 2 and 4 number of passes exhibited only the austenite phase. As clearly evident from the Fig. 7(a), martensitic peaks were observed for the severely peened reference samples with 22 and 42 number of passes. This can be attributed to heavy plastic deformation caused due to severe bombardment of shot peening media leading to deformation induced phase transformation [32,33]. This phase transformation could be dominated by the direct γ (austenite) to α′ (martensite) as previously reported by Liu et al. [15]. The AM samples did not have martensitic

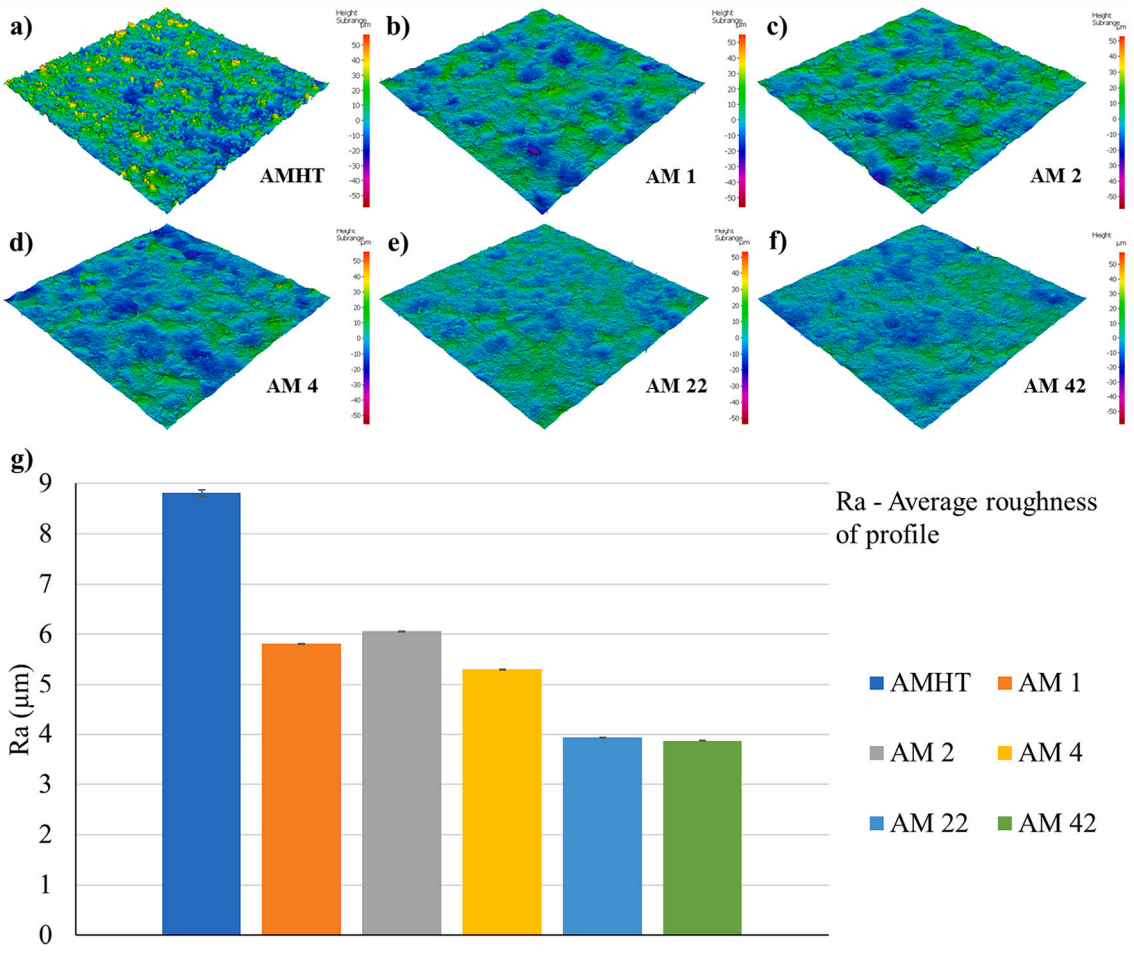

Fig. 6. a-f) 3D topographic images of AM samples; g) Surface roughness of the reference samples derived from the corresponding topographic images.

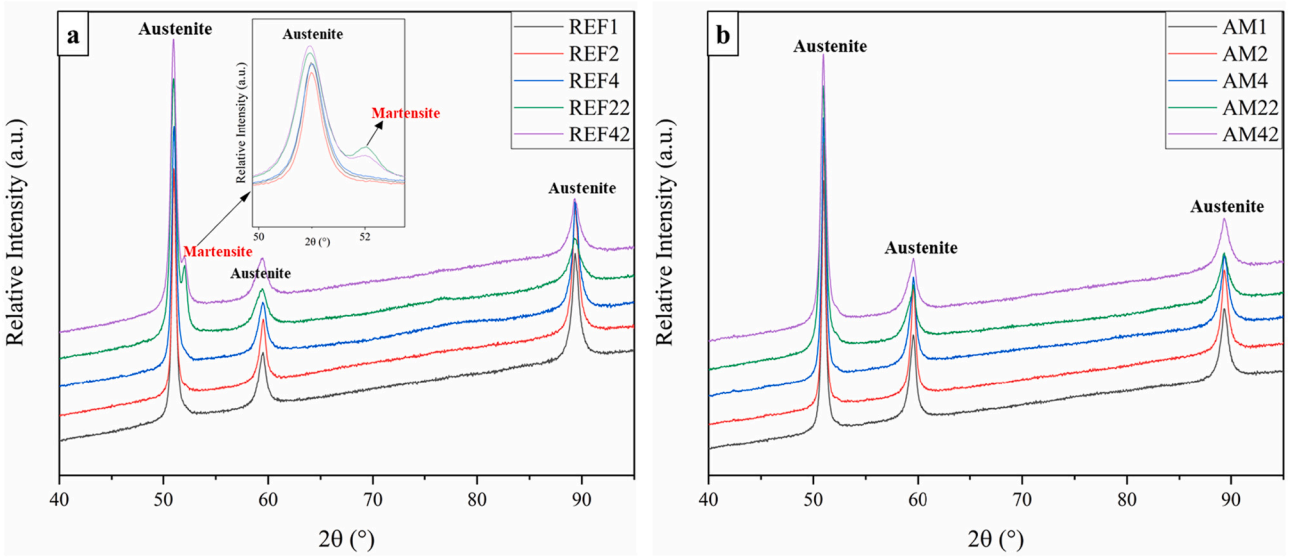

Fig. 7. Crystallographic phases detected from XRD measurements for the shot peened a) Reference samples; b) AM samples.

peaks even for the severely peened samples. This could be attributed to strongly oriented grain structure in SLM built 316 L which could be relatively more resistant to plastic deformation than the reference samples. The resistance to plastic deformation in AM samples is also evident from the relatively lower grain refinement depth of the SSP samples than in reference samples (refer Fig. 10(e-f) and Fig. 11(e-f)).

3.3.2. *Residual stress depth profiles*

The residual stresses in un-peened and shot peened reference samples on surface and along the depth are depicted in Fig. 8(a-b). The error bars are mentioned in the figure, and it is worthwhile to mention that the maximum deviation for the reference samples was ±74.2 MPa from the measured value. It is evident from the figure that shot peening induced compressive residual stresses on the surface and beneath in all the samples. Overall, the compressive residual stresses kept increasing to certain a depth after which the stresses again reduced. It can be seen from the Fig. 8(a-b) that REF 2 has lesser compressive stresses when compared to REF 1. This could be attributed to different nozzle speeds

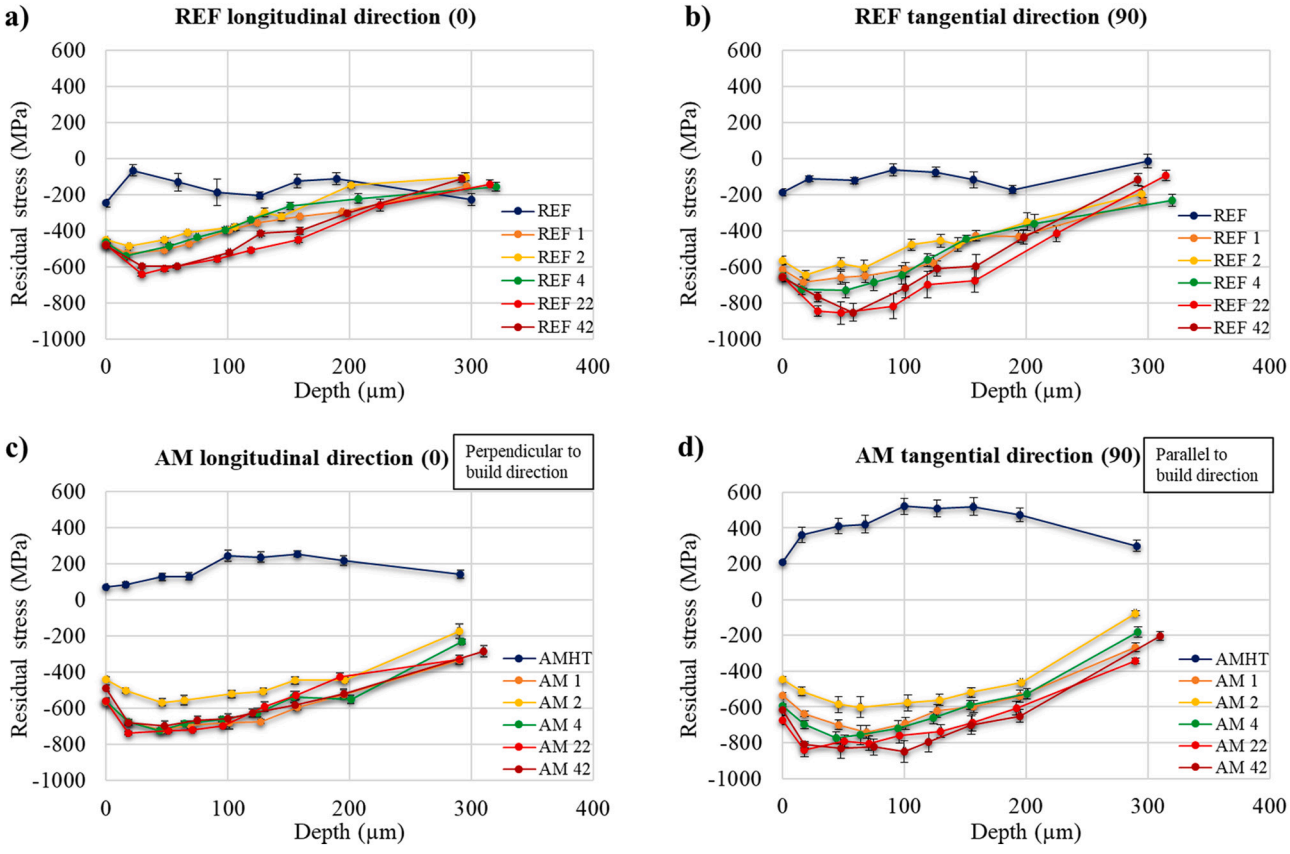

Fig. 8. Residual stress depth profiles in longitudinal (0) and tangential (90) direction respectively a, b) Reference samples; b, c) AM samples.

used during the shot peening. REF 2 was peened with 150 mm/s while REF 1 with 50 mm/s. Faster nozzle speed reduces exposure time of nozzle and thereby peening media to sample surface. Therefore, for REF 2, corresponding number of passes for 50 mm/s speed would be 0.67 instead of 2 (refer Table 2). This makes REF 1 relatively more severe when compared to REF 2. A careful observation also reveals presence of relatively high compressive surface residual stresses with increasing in number of passes. For e.g., REF 2 had compressive residual stress of −565.3 MPa on surface along tangential (90) direction while REF 42 had −657.7 MPa.

The effect of SSP on residual stress behavior of REF 22 and REF 42 can be clearly seen from Fig. 8(a-b). Both the samples have compressive residual stresses of more −500 MPa along the longitudinal direction and − 700 MPa along tangential direction up to 100 μm depth. Furthermore, even up to 200 μm depth, compressive residual stress of −300 MPa along the longitudinal direction and − 400 MPa along tangential direction were observed. This strengthens the understanding of SSP inducing larger residual stresses deeper into the sample than the conventional peening. Previously Bagherifard et al. [14]and Liu et al. [15] have reported similar response of AISI 316 L and 304 stainless steels when subjected to SSP.

The residual stresses in un-peened and shot peened AM samples on surface and along the depth are depicted in Fig. 8(c-d). The error bars are mentioned in the figure, and it is worthwhile to mention that the maximum deviation for the AM samples was ±60.5 MPa from the measured value. The tangential measurement direction (90) corresponds to building direction of the AM samples (refer Fig. 1). Shot peening induced compressive residual stresses on surface and beneath in all the samples both in longitudinal (0) as well as tangential direction (90). Overall, considering both the stress directions, sample AM 2 exhibited the lowest compressive residual stress when compared to the AM 1 and AM 4. This can be attributed to different nozzle speed used during the shot peening as explained earlier. The order of severity was AM 2 > AM 1 > AM 4 when corresponding number of passes are calculated for 50 mm/s (refer Table 2).

The SSP has induced larger compressive residual stresses deeper into the sample when compared to that of AM 1, AM 2, and AM 4 (refer Fig. 8 (d)). REF 22 and REF 42 had compressive residual stresses of more than −750 MPa up to 100 μm and more than −600 MPa up to 200 μm depth. The defect density in SLM built 316 L is more in the vicinity of surface [20–22]. Having these larger and deeper compressive stresses near the surface could facilitate the improved fatigue life of the components.

To summarize, similar residual stress behavior was observed for reference as well as for AM samples when subjected to shot peening. The peening induced compressive residual stresses on the surface and beneath. Furthermore, The SSP induced higher compressive residual stresses relatively deeper into the surface which are essential in improving the fatigue performance. It is worthwhile to mention the that maximum longitudinal compressive residual stress depth was observed for AM 316 L samples compared to REF 316 L samples. This could be attributed to the already present tensile residual stresses in AM 316 L unlike the REF 316 L. Previously, Zhan et al. [34] reported that increase in the compressive residual stresses after shot peening was directly proportional to the prestress state of the samples. More the prestressed sample, more will be the compressive residual stresses after shot peening. The AM 316 L samples had larger longitudinal compressive residual stresses as that of REF 316 L after shot peening which resulted from larger elastic recovery after the prestressed tensile stress release.

The full width half maximum (FWHM) plots for the reference as well as AM samples are indicated in Fig. 9(a) and (b) respectively. It is worthwhile to mention that the error bars were small, and range was ±0.05 to ±0.27. Visually, there is no significant difference between the FWHM behavior of REF and AM samples. The FWHM values on the surface are minimum for the sample with 2 number of passes. That can be attributed to the lowest corresponding number of passes of 0.67 for the 50 mm/s nozzle speed (refer Table 2). The FWHM values seem to have increased with higher number of passes. This can be attributed to an effect of induced surface hardening on the near surface areas due to shot peening. Furthermore, the presence of transformed martensite in REF SSP samples could have also affected the FWHM values. The FWHM values kept decreasing with depth and reached the values of bulk material at the depth of~ 300 μm.

3.4. EBSD measurements

3.4.1. Reference samples

EBSD inverse pole figure (IPF) maps acquired with 70 nm step size of the un-peened as well as shot peened reference samples are presented in Fig. 10(a-f). The difference between deformed grain regions among the samples can be visualized from the IPF maps. The smallest possible step size was used in order to resolve as many tiny, deformed grains near surface as possible. Use of smaller step size enables higher indexing success while reducing the amount of zero solutions [15]. The undeformed surface can be clearly seen for the un-peened REF sample (Fig. 10(a)). Shot peening with 1, 2 and 4 number of passes resulted in deformation of grains near the surface. Bombardment of shot peening media caused plastic deformation and hence grain refinement near the surface. The grain refinement depth of 10–15 μm was observed with 1 and 2 passes and it increased to 20–30 μm with 4 number of passes. Furthermore, subjecting the samples to SSP with 22 and 42 number of

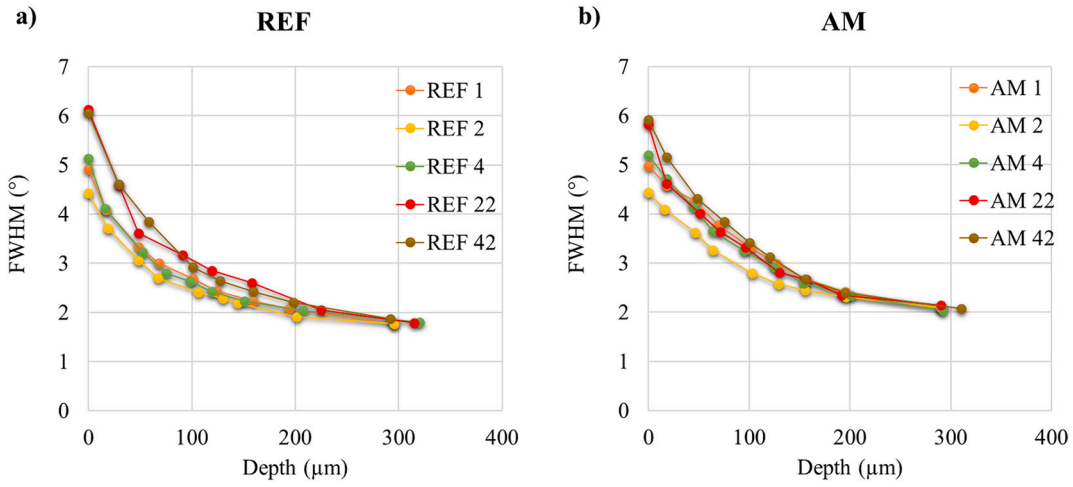

Fig. 9. FWHM values as a function of distance from the surface for a) Reference samples; b) AM samples.

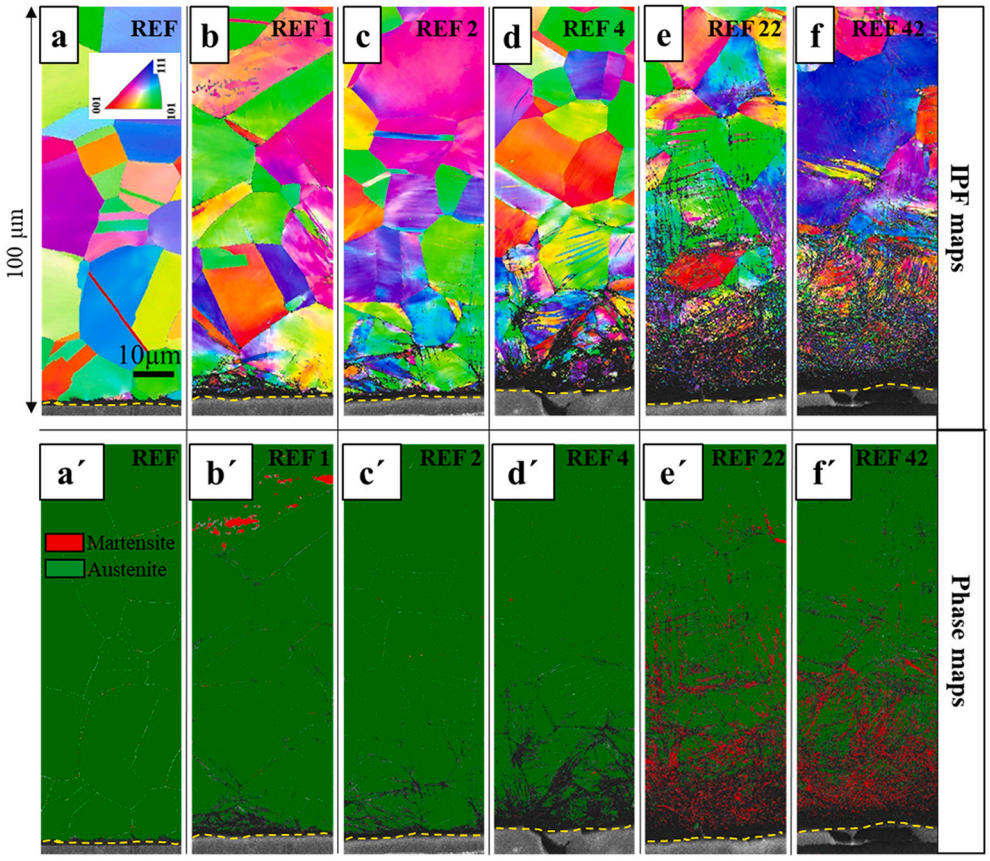

Fig. 10. a-f) Inverse pole figure (IPF) maps of reference samples; a´-f) Phase maps of reference samples. The green and red colour in the phase maps correspond to austenite and martensite respectively. The sample surface zone is indicated by dashed yellow line.

passes resulted in even higher grain refinement depths. It is evident from the figure that the grain refinement depth of 50–80 µm was achieved with SSP. A careful observation shows the smallest grains near the topmost surface and the grain size gradually increases as the depth increases into the bulk material. Bagherifard et al. [14] has reported presence of nano and submicron sized grains near the very surface of severely peened AISI 316 L samples.

The corresponding EBSD phase maps of the un-peened as well as peened reference samples are presented in Fig. 10(a´-f). The green colour represents austenite while martensite is represented by red colour. It is worthwhile to mention that in present study BCC ferrite is considered as martensite due to limited angular resolution of the EBSD system. The used approach is consistent with previously used approach [14]. Presence of transformed martensite can be clearly seen near the surface in the SSP samples with 22 and 42 number of passes (Fig. 10(e´-f)). This can be attributed to the highest localized strain near surface, induced due to sever bombardment of shot peening media. Furthermore, a small amount of martensite was observed in REF 1 and REF 4 samples which is consistent with previous findings [14]. There is a uniform layer of transformed martensite up to 15 µm from the surface of SSP treated samples. At the higher depths, the martensite layer becomes random, and some traces of martensite were present even at the depth of 60–80 µm from the surface. The grain refinement depth and transformation of martensite resulted in significant increase in hardness values near surface (refer Fig. 12(a)). Previously, transformation of austenite to martensite when 316 L and 304 stainless steels samples were subjected to shot peening was confirmed by Bagherifard et al. [14] and Liu et al. [15] respectively.

3.4.2. AM samples

IPF maps of the un-peened as well as peened AM samples presented in Fig. 11(a-f). Similar step size of 70 nm was used to obtain comparable EBSD maps. The un-deformed surface of the AMHT sample can be clearly seen from the Fig. 11(a). Shot peening with 1, 2 and 4 passes resulted in deformation of grains near surface which can be visualized from the Fig. 11(b-d). Shot peening caused deformation on surface due to bombardment of shot peening media. The difference in grain refinement depth among the samples can be clearly seen from the Fig. 11(b-f). The grain deformation depth of 10–25 µm was achieved with 1, 2 and 4 number of passes. The grain deformation depth seems to have increased slightly with 4 number of passes that that of 1 and 2. However, a clear differentiation cannot be made visually and hence the range is stated. SSP with 22 and 42 number of passes resulted in higher grain deformation depth of 40–50 µm was observed. This can be attributed to plastic deformation and hence grain deformation occurred due to severe bombardment of shot peening media.

The corresponding phase maps derived from EBSD data of AM sample are shown in Fig. 11(a´-f). The green colour represents austenite and the red colour probably corresponds to BCC ferrite phase and not the martensite. It is evident from Fig. 7(b) that martensite was not present in any of the shot peened AM samples. Furthermore, previous reports [35–37] also confirm the presence of ferrite phase in the SLM built austenitic 316 L. The presence of this ferrite phase could be detrimental to the corrosion response of the SLM built 316 L [35]. A clear observation reveals presence of relatively more ferrite phase near the surface of AMHT sample. Therefore, shot peening becomes even more critical to enhance the corrosion as well as stress corrosion susceptibility of the AM components by improving surface properties. Shot peening seemingly eliminated the presence of ferrite near the surface just with 1, 2 and 4 number of passes. However, the presence of transformed martensite was not detected in the SSP treated AM samples even with 22 and 42 number of passes Fig. 11(e´-f).

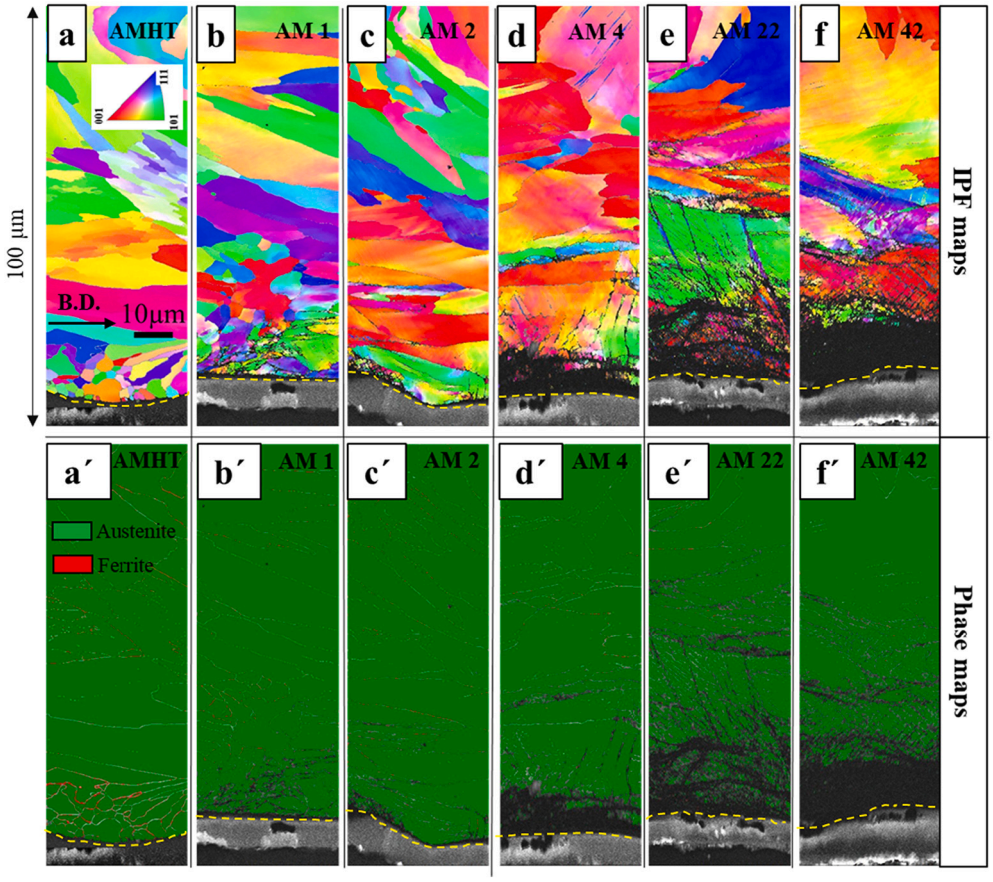

Fig. 11. a-f) Inverse pole figure (IPF) maps of the AM samples; a′-f′) Phase maps of AM samples. The green and red colour in the phase maps correspond to austenite and ferrite respectively. The sample surface zone is indicated by dashed yellow line.

To summarize, shot peening resulted in grain refinements in both REF as well as AM samples. However, the grain refinement depth of the SSP was slightly lower in AM samples (40–50 µm) when compared to that of REF samples (60–80 µm). This could be attributed to relatively strong texture possessed by the AM samples along the building direction making the grains more resisting for deformation. In addition to strong texture, AM samples have very fine substructure in the size range of a few microns unlike Reference samples. Such fine substructures cloud also resist the deformation by SSP. Furthermore, the SSP REF samples were characterized by presence of transformed martensite unlike the SSP AM samples. This strengthens the understanding of AM built components behaving differently to post processing treatments when compared to the conventionally manufactured components.

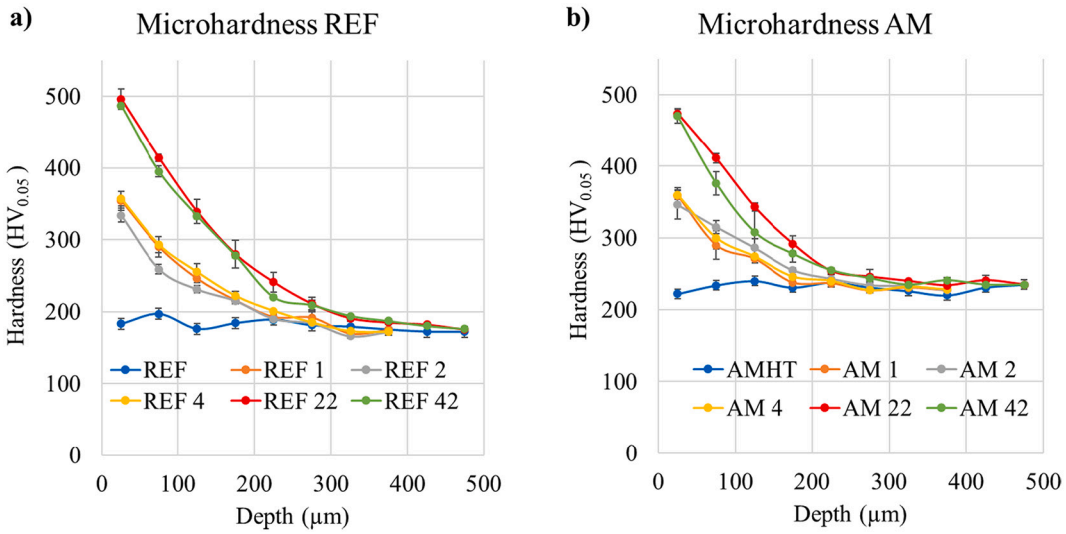

Fig. 12. Microhardness values along depth of a) Reference samples; b) AM samples.

3.5. Microhardness

The measured microhardness values along depth of the shot peened reference and AM samples are depicted in Fig. 12(a) and (b) respectively. The three repeated hardness profiles were similar and only one of them per sample is indicated on the plot for brevity. The un-peened REF sample had an average hardness of 183 ± 7.8 HV. Shot peening with 1, 2 and 4 number of passes increased harness values in the range of 330–360 HV. This 90% increase in the hardness near surface can be attribute to the work hardening caused during shot peening. Furthermore, SSP with 22 and 42 number of passes increased hardness values in the range of 480–500 HV near surface. This tremendous 160% increase in the hardness can be attributed to work hardening along with grain refinement during SSP. The grain refinement can be clearly seen from Fig. 10(é-f). Furthermore, the transformation of austenite to martensite on the near surface areas also contributes to increased hardness (refer Fig. 10(é-f)). The shot peening induced hardness depth is around 275–325 μm after which the harness values reach around the base material hardness of 183 HV.

The un-peened AMHT sample had an average hardness of 230 ± 6.5 HV. The hardness of SLM built 316 L could be affected by processes parameters such as scanning speed, layer thickness and orientation. Lin et al. [31] reported increase in hardness up to certain scanning speed followed by decrease in values. Furthermore lower layer thickness as well as 90° orientation was reported beneficial for achieving better hardness values by Saxena et al. [38]. The applied annealing protocol (600 °C, 2 h) usually does not affect the hardness of as-built SLM 316 L as the complex cellular microstructure remains unaffected at 600 °C [39,40]. The shot peening with 1, 2 and 4 number of passes improved hardness near surface in the range of 340–360 HV. This 50% increase in the hardness near surface could be attributed to the work hardening caused by shot peening. Furthermore, the hardness increased in the range of 470–480 HV when subjected to SSP with 22 and 42 number of passes. This 108% increase in the hardness could be attributed to further work hardening as well as grain refinement in near surface areas. The hardness affected depth for AM samples was in the range of 225–275 μm after which it reached to the base hardness of 230 HV (Refer Fig. 12(b)).

To summarize, SSP induced higher hardness values in both the REF and AM samples. The hardness of REF samples was improved by 160% compared to base material while that of AM sample was increased by 108%. This can be explained by the transformation of austenite to martensite in near surface areas of REF samples unlike AM samples. Also, the lesser hardness affected depth in AM samples compared to REF samples could be attributed to relatively more shallow grain refinement depth achieved due to SSP.

4. Summary and conclusions

SSP response of conventionally manufactured 316 L have been studied and is well understood. However, SSP response of AISI 316 L AM samples was not fully explored. This research gap was addressed by investigating the SSP treated AM samples in the present study. Furthermore, severely shot peened reference (conventionally manufactured 316 L) specimens were also investigated to obtain comparable response. The comprehensive characterization comprised of residual stress behavior, surface topography, grain refinement, phase identification and microhardness led to following findings:

- The roughness and topography response of reference and AM samples when subjected to shot peening relied on the starting surface of the respective samples. The un-peened REF sample was relatively smooth. First, the shot peening increased waviness and roughness while SSP reduced roughness values slightly. The un-peened AMHT samples were relatively rough and hence, first shot peening reduced the roughness while SSP again reduced it even more. The reduced roughness values in both the AM and REF after SSP can be attributed to severe bombardment of shot peening media slightly evening out the surface.
- Similar residual stress behavior was observed for both the reference and AM samples subjected to shot peening. SSP induced higher compressive stresses relatively deeper into the sample which are beneficial for improving the fatigue as well as stress corrosion cracking performance.
- The SSP induced grain refinement relatively deeper into the sample in both the reference and AM samples. However, the depth was lower in AM samples when compared to the reference ones. Furthermore, the original austenitic phase was transformed to martensite when reference samples were subjected to SSP while no phase transformation was observed in AM samples. These differences strengthen the understanding of different behavior of AM samples as that of conventionally manufactured samples when subjected identical post processing conditions because of different processing conditions, distinct microstructures, etc.
- Microhardness of reference as well as AM samples increased significantly near surface when subjected to SSP. Two and a half times increase in near surface hardness values of reference samples when compared to two times increase of AM samples could be attributed the higher grain refinement depths as well as transformation of austenite to martensite in the top layers.

To conclude, the results indicate that SSP induced higher and deeper compressive residual stresses, caused deeper grain refinement, increased hardness values near the surface and improved the surface roughness of AM samples. With such beneficial surface and subsurface structural improvements, it can be commented that SSP has high potential to facilitate the improvement of fatigue life as well as stress corrosion cracking resistance in the AM samples and thus ensuring their usability in wide range of different applications. Authors have planned to study and report the aforementioned fatigue and stress corrosion cracking tests in the future publications.

Funding

This research was funded by Association of Finnish Steel and Metal Producers, grant numbers 750 and 1475. It was also supported by European Union (European Regional Development Fund, Council of Oulu Region) for the “Hybridi” grant number A73071 and “M3D” grant number A77901.

Data availability

The raw/processed data required to reproduce these findings cannot be shared at this time as the data also forms part of an ongoing study.

CRediT authorship contribution statement

Tejas Gundgire: Conceptualization, Formal analysis, Investigation, Visualization, Writing – original draft, Writing – review & editing. **Tuomas Jokiaho:** Conceptualization, Investigation, Writing – review & editing. **Suvi Santa-aho:** Conceptualization, Writing – review & editing. **Timo Rautio:** Conceptualization, Writing – review & editing. **Antti Järvenpää:** Writing – review & editing, Supervision. **Minnamari Vippola:** Conceptualization, Writing – review & editing, Supervision.

Declaration of Competing Interest

The authors declare that they have no known competing financial interests or personal relationships that could have appeared to influence the work reported in this paper.

Data availability

The raw/processed data required to reproduce these findings cannot be shared at this time as the data also forms part of an ongoing study.

Acknowledgements

SEM and EBSD studies made use of Tampere Microscopy Center facilities at Tampere University.

References

[1] J. Gausemeier, N. Echterhoff, M. Wall, Thinking ahead the future of additive manufacturing – innovation roadmapping of required advancements, Univ. Paderborn Direct Manuf. Res. Cent. (2013) 110 [Online]. Available: http://www.hni.uni-paderborn.de/en/pe.
[2] M. Attaran, The rise of 3-D printing: the advantages of additive manufacturing over traditional manufacturing, Bus. Horiz. 60 (5) (2017) 677–688, https://doi.org/10.1016/j.bushor.2017.05.011.
[3] N. Haghdadi, M. Laleh, M. Moyle, S. Primig, Additive manufacturing of steels: a review of achievements and challenges, J. Mater. Sci. 56 (1) (2021) 64–107, https://doi.org/10.1007/s10853-020-05109-0.
[4] F. Bartolomeu, et al., 316L stainless steel mechanical and tribological behavior—a comparison between selective laser melting, hot pressing and conventional casting, Addit. Manuf. 16 (2017) 81–89, https://doi.org/10.1016/j.addma.2017.05.007.
[5] R.B. Song, J.Y. Xiang, D.P. Hou, Characteristics of mechanical properties and microstructure for 316L austenitic stainless steel, J. Iron Steel Res. Int. 18 (11) (2011) 53–59, https://doi.org/10.1016/S1006-706X(11)60117-9.
[6] S. Santa-Aho, et al., Additive manufactured 316l stainless-steel samples: microstructure, residual stress and corrosion characteristics after post-processing, Metals (Basel). 11 (2) (2021) 1–16, https://doi.org/10.3390/met11020182.
[7] C. Li, Z.Y. Liu, X.Y. Fang, Y.B. Guo, Residual stress in metal additive manufacturing, Procedia CIRP 71 (2018) 348–353, https://doi.org/10.1016/j.procir.2018.05.039.
[8] J.H. Robinson, I.R.T. Ashton, E. Jones, P. Fox, C. Sutcliffe, The effect of hatch angle rotation on parts manufactured using selective laser melting, Rapid Prototyp. J. 25 (2) (2019) 289–298, https://doi.org/10.1108/RPJ-06-2017-0111.
[9] K. Kempen, B. Vrancken, S. Buls, L. Thijs, J. Van Humbeeck, J.P. Kruth, Selective laser melting of crack-free high density M2 high speed steel parts by baseplate preheating, J. Manuf. Sci. Eng. Trans. ASME 136 (6) (2014) 1–6, https://doi.org/10.1115/1.4028513.
[10] P. Mercelis, J.P. Kruth, Residual stresses in selective laser sintering and selective laser melting, Rapid Prototyp. J. 12 (5) (2006) 254–265, https://doi.org/10.1108/13552540610707013.
[11] H. Kim, Y. Lin, T.L.B. Tseng, A review on quality control in additive manufacturing, Rapid Prototyp. J. 24 (3) (2018) 645–669, https://doi.org/10.1108/RPJ-03-2017-0048.
[12] V. Cruz, Q. Chao, N. Birbilis, D. Fabijanic, P.D. Hodgson, S. Thomas, Electrochemical studies on the effect of residual stress on the corrosion of 316L manufactured by selective laser melting, Corros. Sci. 164 (October) (2019) 108314, 2020, https://doi.org/10.1016/j.corsci.2019.108314.
[13] G.H. Farrahi, J.L. Lebrijn, D. Couratin, Effect of shot peening on residual stress and fatigue life of a spring steel, Fatigue Fract. Eng. Mater. Struct. 18 (2) (1995) 211–220, https://doi.org/10.1111/j.1460-2695.1995.tb00156.x.
[14] S. Bagherifard, S. Slawik, I. Fernández-Pariente, C. Pauly, F. Mücklich, M. Guagliano, Nanoscale surface modification of AISI 316L stainless steel by severe shot peening, Mater. Des. 102 (2016) 68–77, https://doi.org/10.1016/j.matdes.2016.03.162.
[15] H. Liu, Y. Wei, C.K.I. Tan, D.T. Ardi, D.C.C. Tan, C.J.J. Lee, XRD and EBSD studies of severe shot peening induced martensite transformation and grain refinements in austenitic stainless steel, Mater. Charact. 168 (August) (2020), 110574, https://doi.org/10.1016/j.matchar.2020.110574.
[16] W. Shi, P. Wang, Y. Liu, Y. Hou, G. Han, Properties of 316L formed by a 400 W power laser selective laser melting with 250 μm layer thickness, Powder Technol. 360 (2020) 151–164, https://doi.org/10.1016/j.powtec.2019.09.059.
[17] G. Dursun, S. Ibekwe, G. Li, P. Mensah, G. Joshi, D. Jerro, Influence of laser processing parameters on the surface characteristics of 316L stainless steel manufactured by selective laser melting, Mater. Today Proc. 26 (2019) 387–393, https://doi.org/10.1016/j.matpr.2019.12.061.
[18] J.-P. Kruth, E. Yasa, J. Deckers, Roughness improvement in selective laser melting, Proc. 3rd Int. Conf. Polym. Mould. Innov. (2008) 170–183.
[19] T. Rautio, A. Hamada, J. Kumpula, A. Järvenpää, T. Allam, Enhancement of electrical conductivity and corrosion resistance by silver shell-copper core coating of additively manufactured AlSi10Mg alloy, Surf. Coat. Technol. 403 (September) (2020), 126426, https://doi.org/10.1016/j.surfcoat.2020.126426.
[20] S. Beretta, S. Romano, A comparison of fatigue strength sensitivity to defects for materials manufactured by AM or traditional processes, Int. J. Fatigue 94 (2017) 178–191, https://doi.org/10.1016/j.ijfatigue.2016.06.020.
[21] A. Yadollahi, N. Shamsaei, Additive manufacturing of fatigue resistant materials: challenges and opportunities, Int. J. Fatigue 98 (2017) 14–31, https://doi.org/10.1016/j.ijfatigue.2017.01.001.
[22] S. Dryepondt, P. Nandwana, P. Fernandez-Zelaia, F. List, Microstructure and high temperature tensile properties of 316L fabricated by laser powder-bed fusion, Addit. Manuf. 37 (May) (2020) 101723, 2021, https://doi.org/10.1016/j.addma.2020.101723.
[23] J.M. Champaigne, Almen gage calibration, Shot Peen. (September) (2006) 108–113, https://doi.org/10.1002/3527606580.ch15.
[24] T. Rautio, M. Jaskari, T. Gundgire, T. Iso-Junno, M. Vippola, A. Järvenpää, The effect of severe shot peening on fatigue life of laser powder bed fusion manufactured 316L stainless steel, Materials (Basel). 15 (10) (2022) 3517, https://doi.org/10.3390/ma15103517.
[25] O. Sfs-standardi, Tampereen Teknillinen Yliopisto, no. Malminkatu 34, 2022.
[26] R. Alkaisee, R.L. Peng, Influence of layer removal methods in residual stress profiling of a shot peened steel using X-ray diffraction, Adv. Mater. Res. 996 (2014) 175–180, https://doi.org/10.4028/www.scientific.net/AMR.996.175.
[27] F. Valiorgue, G. Kermouche, V. Lacaille, S. Zuchiatti, J. Rech, Electrolytic polishing influence on residual stresses measurements, 7ème Assises MUGV2012 (October) (2012) 16–18.
[28] S. Kheiri, H. Mirzadeh, M. Naghizadeh, Tailoring the microstructure and mechanical properties of AISI 316L austenitic stainless steel via cold rolling and reversion annealing, Mater. Sci. Eng. A 759 (May) (2019) 90–96, https://doi.org/10.1016/j.msea.2019.05.028.
[29] B. Song, et al., Differences in microstructure and properties between selective laser melting and traditional manufacturing for fabrication of metal parts: a review, Front. Mech. Eng. 10 (2) (2015) 111–125, https://doi.org/10.1007/s11465-015-0341-2.
[30] A. Townsend, N. Senin, L. Blunt, R.K. Leach, J.S. Taylor, Surface texture metrology for metal additive manufacturing: a review, Precis. Eng. 46 (2016) 34–47, https://doi.org/10.1016/j.precisioneng.2016.06.001.
[31] K. Lin, et al., Selective laser melting processing of 316L stainless steel: effect of microstructural differences along building direction on corrosion behavior, Int. J. Adv. Manuf. Technol. 104 (5–8) (2019) 2669–2679, https://doi.org/10.1007/s00170-019-04136-9.
[32] G.B. Olson, M. Cohen, A mechanism for the strain-induced martensitic transformations, J. Less-Common Met. 28 (1972) 107–118.
[33] H. Hotz, B. Kirsch, T. Zhu, M. Smaga, T. Beck, J.C. Aurich, Surface layer hardening of metastable austenitic steel – comparison of shot peening and cryogenic turning, J. Mater. Res. Technol. 9 (6) (2020) 16410–16422, https://doi.org/10.1016/j.jmrt.2020.11.109.
[34] K. Zhan, C.H. Jiang, V. Ji, Effect of prestress state on surface layer characteristic of S30432 austenitic stainless steel in shot peening process, Mater. Des. 42 (2012) 89–93, https://doi.org/10.1016/j.matdes.2012.05.053.
[35] T. Kurzynowski, K. Gruber, W. Stopyra, B. Kuźnicka, E. Chlebus, Correlation between process parameters, microstructure and properties of 316 L stainless steel processed by selective laser melting, Mater. Sci. Eng. A 718 (January) (2018) 64–73, https://doi.org/10.1016/j.msea.2018.01.103.
[36] F.C. Pinto, I.R. Souza Filho, M.J.R. Sandim, H.R.Z. Sandim, Defects in parts manufactured by selective laser melting caused by δ-ferrite in reused 316L steel powder feedstock, Addit. Manuf. 31 (June) (2019) 100979, 2020, https://doi.org/10.1016/j.addma.2019.100979.
[37] K. Saeidi, X. Gao, Y. Zhong, Z.J. Shen, Hardened austenite steel with columnar subgrain structure formed by laser melting, Mater. Sci. Eng. A 625 (2015) 221–229, https://doi.org/10.1016/j.msea.2014.12.018.
[38] P. Saxena, H. Gajera, D. Shah, N. Pancholi, Effect of SLM process parameters on hardness and microstructure of stainless steel 316 material, Mater. Today Proc. (xxxx) (2021), https://doi.org/10.1016/j.matpr.2021.09.144.
[39] M.S.I.N. Kamariah, W.S.W. Harun, N.Z. Khalil, F. Ahmad, M.H. Ismail, S. Sharif, Effect of heat treatment on mechanical properties and microstructure of selective laser melting 316L stainless steel, IOP Conf. Ser. Mater. Sci. Eng. 257 (1) (2017), https://doi.org/10.1088/1757-899X/257/1/012021.
[40] O.O. Salman, C. Gammer, A.K. Chaubey, J. Eckert, S. Scudino, Effect of heat treatment on microstructure and mechanical properties of 316L steel synthesized by selective laser melting, Mater. Sci. Eng. A 748 (January) (2019) 205–212, https://doi.org/10.1016/j.msea.2019.01.110.